Inorg. Chem. **2004**, *43*, 7083–7093

Tuning of Redox Potentials for the Design of Ruthenium Anticancer Drugs − an Electrochemical Study of [*trans*-$RuCl_4L(DMSO)]^-$ and [*trans*-$RuCl_4L_2]^-$ Complexes, where L = Imidazole, 1,2,4-Triazole, Indazole

Erwin Reisner,[†,‡] Vladimir B. Arion,*[,‡] M. Fátima C. Guedes da Silva,[†,§] Roman Lichtenecker,[‡] Anna Eichinger,[‡] Bernhard K. Keppler,*[,‡] Vadim Yu. Kukushkin,[||] and Armando J. L. Pombeiro*[,†]

Centro de Química Estrutural, Complexo I, Instituto Superior Técnico, Av. Rovisco Pais, 1049-001 Lisbon, Portugal, Institute of Inorganic Chemistry, University of Vienna, Währingerstrasse 42, A-1090 Vienna, Austria, Universidade Lusófona de Humanidades e Tecnologias, Av. Campo Grande 376, 1749-024 Lisbon, Portugal, and Department of Chemistry, St. Petersburg State University, 198504 Stary Petergof, Russian Federation

Received April 23, 2004

The electrochemical behavior of [*trans*-$RuCl_4L(DMSO)]^-$ (**A**) and [*trans*-$RuCl_4L_2]^-$ (**B**) [L = imidazole (Him), 1,2,4-triazole (Htrz), and indazole (Hind)] complexes has been studied in DMF, DMSO, and aqueous media by cyclic voltammetry and controlled potential electrolysis. They exhibit one single-electron Ru^{III}/Ru^{II} reduction involving, at a sufficiently long time scale, metal dechlorination on solvolysis, as well as, in organic media, one single-electron reversible Ru^{III}/Ru^{IV} oxidation. The redox potential values are interpreted on the basis of the Lever's parametrization method, and particular forms of this linear expression (that relates the redox potential with the ligand E_L parameter) are proposed, for the first time, for negatively (1–) charged complexes with the $Ru^{III/II}$ redox couple center in aqueous phosphate buffer (pH 7) medium and for complexes with the $Ru^{III/IV}$ couple in organic media. The E_L parameter was estimated for indazole showing that this ligand behaves as a weaker net electron donor than imidazole or triazole. The kinetics of the reductively induced stepwise replacement of chloride by DMF were studied by digital simulation of the cyclic voltammograms, and the obtained rate constants were shown to increase with the net electron donor character (decrease of E_L) of the neutral ligands (DMSO < indazole < triazole < imidazole) and with the basicity of the ligated azole, factors that destabilize the Ru^{II} relative to the Ru^{III} form of the complexes. The synthesis and characterization of some novel complexes of the **A** and **B** series are also reported, including the X-ray structural analyses of (Ph_3PCH_2Ph)[*trans*-$RuCl_4$(Htrz)(DMSO)], $[(Ph_3P)_2N]$[*trans*-$RuCl_4$(Htrz)(DMSO)], (H_2ind)-[*trans*-$RuCl_4$(Hind)(DMSO)], and $[(Hind)_2H]$[*trans*-$RuCl_4(Hind)_2$].

Introduction

The search for novel ruthenium-based antitumor drugs has been stimulated by clinical success of metal-containing drugs in general[1−4] and, in particular, by recent reaching of clinical trials of two ruthenium complexes, i.e., (H_2im)[*trans*-$RuCl_4$-(Him)(DMSO)] (NAMI-A, Him = imidazole),[5−10] as an efficient anti-metastatic drug, and (H_2ind)[*trans*-$RuCl_4$-

* Authors to whom correspondence should be addressed. E-mail: arion@ap.univie.ac.at (V.B.A.); keppler@ap.univie.ac.at (B.K.K.); pombeiro@ist.utl.pt (A.J.L.P.)

† Centro de Química Estrutural, Complexo I, Instituto Superior Técnico.

‡ Institute of Inorganic Chemistry, University of Vienna.

§ Universidade Lusófona de Humanidades e Tecnologias.

|| Department of Chemistry, St. Petersburg State University.

(1) Wong, E.; Giandomenico, C. M. *Chem. Rev.* **1999**, *99*, 2451−2466.
(2) Rosenberg, B.; VanCamp, L. *Cancer Res.* **1970**, *30*, 1799−1802.
(3) Rosenberg, B.; VanCamp, L.; Krigas, T. *Nature* **1965**, *205*, 698−699.
(4) Guo, Z.; Sadler, P. J. *Angew. Chem., Int. Ed.* **1999**, *38*, 1512−1531.
(5) Sava, G.; Gagliardi, R.; Bergamo, A.; Alessio, E.; Mestroni, G. *Anticancer Res.* **1999**, *19*, 969−972.
(6) Bergamo, A.; Gagliardi, R.; Scarcia, B.; Furlani, A.; Alessio, E.; Mestroni, G.; Sava, G. *J. Pharmacol. Exp. Ther.* **1999**, *289*, 559−564.
(7) Sava, G.; Capozzi, I.; Clerici, K.; Gagliardi, G.; Alessio, E.; Mestroni, G. *Clin. Exp. Met.* **1998**, *16*, 371−379.
(8) Bergamo, A.; Cocchietto, M.; Capozzi, I.; Mestroni, G.; Alessio, E.; Sava, G. *Anti-Cancer Drugs* **1996**, *7*, 697−702.
(9) Sava, G.; Clerici, K.; Capozzi, I.; Cocchietto, M.; Gagliardi, R.; Alessio, E.; Mestroni, G.; Perbellini, A. *Anti-Cancer Drugs* **1999**, *10*, 129−138.

10.1021/ic049479c CCC: $27.50
Published on Web 09/21/2004

$(Hind)_2$] (KP1019, Hind = indazole),[11,12] as an anticancer drug that exhibits excellent activity especially against autochtonous colorectal tumors. Moreover, quite recently we observed that both *trans*- and *cis*-isomers of $[RuCl_4(Htrz)_2]^-$ (Htrz = 1,2,4-triazole) exhibit a time-dependent response of three human cell lines, i.e., SW480, HT29 and SK-BR-3, and, in addition, the *trans*-isomer displays a higher antiproliferative activity than the *cis*-species.[13]

Although the mode of antitumor action of the ruthenium(III)-containing species has not yet been established, it was suggested that a mechanism which originates from an *activation by reduction* might be responsible for the activity of NAMI-A and KP1019.[14−17] According to this hypothesis the reduction of the Ru^{III} center would produce more labile, toward substitution, Ru^{II}−Cl species, which would rapidly react with specific sites of proteins altering their activity.[16] Thus, to be active in vivo the Ru^{III} complexes, acting as prodrugs, should possess biologically accessible reduction potentials (from −0.4 to +0.8 V vs NHE).[5,14−16,18]

While the qualitative aspects of the hypothesis of activation by reduction are already well-recognized,[14,15] little was done to systematically investigate the electrochemical behavior of the anticancer agents. To provide a methodological approach on how to tune the Ru^{III}/Ru^{II} redox potential to design prodrugs of the type [*trans*-$RuCl_4L(DMSO)]^-$ (**A**) and [*trans*-$RuCl_4L_2]^-$ (**B**) (L = azole ligand), which could be activated in tumor cells and remain inactive in normal tissues, we performed an electrochemical study of a series of these complexes (Figure 1) where the ligands imidazole, 1,2,4-triazole, and indazole (Figure 2) were chosen due to the good antitumor activity of their corresponding Ru^{III} complexes and their effect on ruthenium redox potential.

The kinetics of the cathodically induced chloride ligand substitution on complexes **A** and **B** were investigated by digital simulation of the cyclic voltammograms and shown to correlate with the basicity of the azo-N atom of the heterocyclic ligand, which provides a useful tool for further design of Ru-based antitumor complexes. In addition, on the basis of the general expression proposed by Lever (eq 1),[19] which assumes an additive contribution to the redox potential of all the ligands (as measured for each of them by the E_L ligand parameter) and in which S_M and I_M are dependent upon the metal and redox couple, the spin state, and the stereochemistry, we have tentatively estimated the E_L parameter for one of the N-ligands of this study (indazole), identified some new products, and predicted the reduction potentials for ruthenium(III) anticancer compounds.

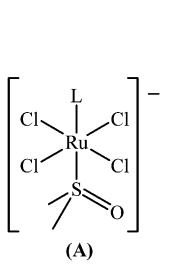

Complex	Counterion	L
A1	H_2im^+	Him
A1a	$Ph_3PCH_2Ph^+$	Him
A2	H_2trz^+	Htrz
A2a	$Ph_3PCH_2Ph^+$	Htrz
A2b	PPN^+	Htrz
A3	H_2ind^+	Hind
A3a	$Ph_3PCH_2Ph^+$	Hind
B1	H_2im^+	Him
B2	H_2trz^+	Htrz
B3	H_2ind^+	Hind
B3a	$(Hind)_2H^+$	Hind
B3b	Na^+	Hind

Figure 1. Anticancer ruthenium(III) complexes of the types **A** [*trans*-$RuCl_4L(DMSO)]^-$, and **B** [*trans*-$RuCl_4L_2]^-$; underlined complexes have been characterized in this work by X-ray crystallography.

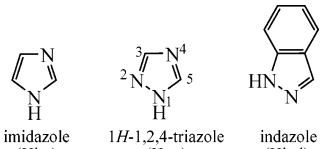

Figure 2. Heterocyclic azole ligands.

$$E = S_M \cdot \sum E_L + I_M \quad (1)$$

Moreover, in pursuit of our interest in the establishment of redox potential−structure relationships in coordination compounds,[20−26] we have extended the application of Lever's equation (eq 1) to the reduction of the negatively (1−) charged Ru^{III} complexes in neutral aqueous phosphate buffer medium, and to the oxidation of such Ru^{III} complexes in an organic medium, by obtaining, for the first time, S_M and I_M for such types of systems. The thus-proposed particular forms of eq 1 can also give a valuable contribution toward the possibility of tuning the redox potentials of Ru^{III} complexes with pharmacological significance.

(10) Sava, G.; Alessio, E.; Bergamo, A.; Mestroni, G. In *Metallopharmaceuticals*; Clarke, M. J., Sadler, P. J., Eds.; Topics in Biological Inorganic Chemistry series, vol. 1; Springer: Berlin, 1999; pp 143−169.
(11) Keppler, B. K.; Lipponer, K. G.; Stenzel, B.; Kratz, F. In *Metal Complexes in Cancer Chemotherapy*; Keppler, B. K., Ed.; VCH: Weinheim, 1993; pp 187−220.
(12) Galanski, M.; Arion, V. B.; Jakupec, M. A.; Keppler, B. K. *Curr. Pharm. Des.* **2003**, *9*, 2078−2089.
(13) Arion, V. B.; Reisner, E.; Fremuth, M.; Jakupec, M. A.; Keppler, B. K.; Kukushkin, V. Yu.; Pombeiro, A. J. L. *Inorg. Chem.* **2003**, *42*, 6024−6031.
(14) Clarke, M. J. *Coord. Chem. Rev.* **2003**, *236*, 209−233, and references therein.
(15) Clarke, M. J.; Zhu, F.; Frasca, D. R. *Chem. Rev.* **1999**, *99*, 2511−2533, and references therein.
(16) Clarke, M. J. *Prog. Clin. Biochem. Med.* **1989**, *10*, 25−39.
(17) Alessio, E.; Balducci, G.; Lutman, A.; Mestroni, G.; Calligaris, M.; Attia, W. M. *Inorg. Chim. Acta* **1993**, *203*, 205−217.
(18) Kirlin, W. G.; Cai, J.; Thompson, S. A.; Diaz, D.; Kavanagh, T. J.; Jones, D. P. *Free Radical Biol. Med.* **1999**, *27*, 1208−1218.
(19) Lever, A. B. P. *Inorg. Chem.* **1990**, *29*, 1271−1285.
(20) Pombeiro, A. J. L. *New J. Chem.* **1997**, *21*, 649−660.
(21) Zang, L.; Guedes da Silva, M. F. C.; Kuznetsov, M. L.; Gamasa, M. P.; Gimeno, J.; Fraústo da Silva, J. J. R.; Pombeiro, A. J. L. *Organometallics* **2001**, *20*, 2782−2793.
(22) Guedes da Silva, M. F. C.; Trzeciak, A. M.; Ziólkowski, J. J.; Pombeiro, A. J. L. *J. Organomet. Chem.* **2001**, *620*, 174−181.
(23) Guedes da Silva, M. F. C.; Fraústo da Silva, J. J. R.; Pombeiro, A. J. L.; Amatore, C.; Verpeaux, J. N. *Inorg. Chem.* **1998**, *37*, 2344−2350.
(24) Almeida, S. S. P. R.; Pombeiro, A. J. L. *Organometallics* **1997**, *16*, 4469−4478.
(25) Pombeiro, A. J. L.; Costa, M. T. A. R. S.; Wang, Y.; Nixon, J. F. *J. Chem. Soc. Dalton Trans.* **1999**, 3755−3758.
(26) Guedes da Silva, M. F. C.; Martins, L. M. D. R. S.; Fraústo da Silva, J. J. R.; Pombeiro, A. J. L. *Collect. Czech. Chem. Commun.* **2001**, *66*, 139−154.

All these results along with the syntheses (**A1a**, **A2**, **A2a**, **A2b**, **A3**, **A3a**, and **B3a**) and structural characterization (**A2a**, **A2b**, **A3**, and **B3a**) for some of the complexes are reported herein.

Experimental Section

Physical Measurements. Elemental analyses were carried out by the Microanalytical Service of the Instituto Superior Técnico in Lisbon or on a Carlo Erba microanalyzer at the Institute of Physical Chemistry of the University of Vienna. Infrared spectra were recorded on a Perkin-Elmer FTIR 2000 spectrometer in KBr pellets (4000−400 cm^{-1}). UV−vis spectra were recorded on a Perkin-Elmer Lambda 9 UV−vis spectrophotometer using samples dissolved in water or methanol. Electrospray ionization mass spectrometry was carried out in methanol with a Bruker Esquire 3000 instrument (Bruker Daltonic, Bremen, Germany). The given *m*/*z* values, originating from the most intense isotopes, were obtained by the mass linearization procedure. Expected and experimental isotope distributions were compared. Melting points were measured on a Kofler-table (Leica Galen III). For TLC, Merck UV 254 SiO_2 plates were used.

Cyclic voltammograms were measured in a two-compartment three-electrode cell using a 1.0-mm-diameter glassy-carbon disk (or a 0.5-mm-diameter platinum disk) working electrode, probed by a Luggin capillary connected to a silver-wire pseudo-reference electrode, and a platinum auxiliary electrode. Measurements were performed by cyclic voltammetry (CV) at room temperature using an EG & G PARC 273A potentiostat/galvanostat. Controlled potential electrolyses (CPE) were carried out in a two-compartment three-electrode cell with a carbon plate working electrode and a platinum gauze counter electrode separated by a glass frit; a Luggin capillary, probing the working electrode, was connected to a silver-wire pseudo-reference electrode. Deaeration of solutions was accomplished by passing a stream of high-purity nitrogen through the solution for 10 min prior to the measurements and then maintaining a blanket atmosphere of nitrogen over the solution during the measurements. The potentials were measured in 0.15 M [$n$$Bu_4N$][$BF_4$]/DMF or DMSO and in 0.2 M phosphate buffer at pH 7 or aqueous 0.2 M KNO_3, using the $[Fe(\eta^5\text{-}C_5H_5)_2]^{0/+}$ ($E_{1/2}^{ox}$ = +0.72 V or +0.68 V vs NHE in DMF or DMSO, respectively),[27,28] or methyl viologen ($E_{1/2}^{ox}$ = −0.44 V[28] vs NHE in water), respectively, as internal standards, and are quoted relative to NHE.

Crystallographic Structure Determination. X-ray diffraction measurements were performed on a Nonius Kappa CCD diffractometer at 120 K. Single crystals were positioned at 30, 30, 35, and 25 mm from the detector, and 376, 389, 488, and 240 frames were measured, each for 100, 100, 70, and 220 s over 2, 1.5, 1.5, and 2° for **A2a**, **A2b**, **A3**, and **B3a**, respectively. The data were processed using the Denzo-SMN software. The structures were solved by direct methods by using the SHELXS-97 package and refined by full-matrix least-squares techniques with SHELXL-97.[29,30] All hydrogens were inserted in calculated positions and refined using a riding model. Drawings were made with ORTEP.[31,32]

Chemicals. Imidazole, 1*H*-1,2,4-triazole, indazole, methyl viologen, (Ph_3PCH_2Ph)Cl, (PPN)Cl, i.e. [$(PPh_3)_2N$]Cl [bis(triphenylphosphine)iminium chloride], ferrocene, and solvents were commercially available from Aldrich and used as purchased.

Synthesis of Complexes. (H_2im)[*trans*-$RuCl_4$(Him)(DMSO)] (**A1**),[33] [$(DMSO)_2H$][*trans*-$RuCl_4(DMSO)_2$],[34] (H_2im)[*trans*-$RuCl_4$(Him)$_2$] (**B1**),[35] (H_2trz)[*trans*-$RuCl_4(Htrz)_2$] (**B2**),[13] (H_2ind)[*trans*-$RuCl_4(Hind)_2$] (**B3**),[36] and Na[*trans*-$RuCl_4(Hind)_2$][37] (**B3b**) were prepared as described elsewhere.

(H_2trz)[*trans*-$RuCl_4$(Htrz)(DMSO)] (A2). 1,2,4-Triazole (2.00 g, 29.0 mmol) was added to [$(DMSO)_2H$][*trans*-$RuCl_4(DMSO)_2$] (1.00 g, 1.8 mmol) in ethanol (96%, 40 mL) and the suspension was vigorously stirred for complete dissolution. The orange mixture was left standing overnight at room temperature. The orange precipitate formed was filtered off, washed with two 10-mL portions of diethyl ether, and dried at room temperature in vacuo. Yield: 0.35 g, 42% based on Ru. Anal. Calcd for $C_6H_{13}N_6Cl_4ORuS$ (M_r = 462.17 g/mol), %: C, 15.66; H, 2.85; N, 18.26; S, 6.97. Found, %: C, 15.71; H, 2.82; N, 18.36; S, 7.21. ESI-MS(-ve), *m*/*z*: 391 [$RuCl_4$(Htrz)(DMSO)]$^-$; 322 [$RuCl_4$(DMSO)]$^-$; 244 [$RuCl_4$]$^-$. mp = 142 °C. TLC on SiO_2, R_f = 0.49 (eluent CH_2Cl_2/MeOH = 70:30). IR spectrum in KBr, selected bands, cm^{-1}: 1115 s, 1083 vs ν(S = O), 432 s ν(Ru − S).

(H_2ind)[*trans*-$RuCl_4$(Hind)(DMSO)] (A3). Indazole (0.47 g, 4.0 mmol) was added to [$(DMSO)_2H$][*trans*-$RuCl_4(DMSO)_2$] (1.12 g, 2.0 mmol) in acetone (30 mL). The mixture was heated at 45 °C over 0.75 h, and allowed to cool to room temperature. The brick-red product formed was filtered off, washed with acetone, and dried at room temperature in vacuo. Yield: 0.60 g, 53% based on Ru. Anal. Calcd for $C_{16}H_{19}N_4Cl_4ORuS$ (M_r = 558.28 g/mol), %: C, 34.42; H, 3.43; N, 10.04; S, 5.74. Found, %: C, 34.46; H, 3.37; N, 9.99; S, 5.86. ESI-MS(-ve), *m*/*z*: 440 [$RuCl_4$(Hind)(DMSO)]$^-$; 322 [$RuCl_4$(DMSO)]$^-$; 244 [$RuCl_4$]$^-$. mp = 170 °C (dec). TLC on SiO_2, R_f = 0.51 (eluent CH_2Cl_2/MeOH = 75:25). IR spectrum in KBr; selected bands, cm^{-1}: 1126 m, 1097 s, 1061 vs ν(S = O), 424 vs ν(Ru − S). Single crystals suitable for X-ray diffraction study were selected directly from the isolated product.

(Ph_3PCH_2Ph)[*trans*-$RuCl_4$L(DMSO)] [L = Him (A1a), Htrz (A2a), Hind (A3a)], and (PPN)[*trans*-$RuCl_4$(Htrz)(DMSO)] (A2b). A solution of (Ph_3PCH_2Ph)Cl (0.09 g, 0.22 mmol) or of (PPN)Cl (0.13 g, 0.22 mmol) in EtOH (96%, 1 mL) was added to (HL)[*trans*-$RuCl_4$L(DMSO)] (0.22 mmol) in H_2O (2 mL) with stirring. The immediately formed powder was filtered off, washed with two 2-mL portions of H_2O, two 2-mL portions of EtOH (96%), and two 2-mL portions of diethyl ether, and dried at room temperature in vacuo. The synthesis of (Ph_3PCH_2Ph)[*trans*-$RuCl_4$(Hind)(DMSO)] (**A3a**) was carried out in ethanol (96%, 8 mL).

(Ph_3PCH_2Ph)[*trans*-$RuCl_4$(Him)(DMSO)] (A1a). Yellow powder. Yield: 0.14 g, 83% based on Ru. Anal. Calcd for $C_{30}H_{32}N_2Cl_4OPRuS$ (M_r = 742.51 g/mol), %: C, 48.53; H, 4.34; N, 3.77; S, 4.32. Found, %: C, 48.57; H, 4.35; N, 3.74; S, 4.34. ESI-MS(-ve), *m*/*z*: 390 [$RuCl_4$(Him)(DMSO)]$^-$; 322 [$RuCl_4$(DMSO)]$^-$; 244 [$RuCl_4$]$^-$. ESI-MS(+ve), 353 (Ph_3PCH_2Ph)$^+$. mp = 191 °C. TLC on SiO_2, R_f = 0.53 (eluent CH_2Cl_2/MeOH = 85:15). IR spectrum in KBr; selected bands, cm^{-1}: 1112 vs, 1063 vs ν(S = O), 421 m ν(Ru − S). UV−vis (MeOH), λ_{max}, nm (ϵ, mM^{-1} cm^{-1}): 466 (0.51), 398 (4.08), 295 (1.20).

(Ph_3PCH_2Ph)[*trans*-$RuCl_4$(Htrz)(DMSO)] (A2a). Yellow powder. Yield: 0.14 g, 88% based on Ru. Anal. Calcd. for $C_{29}H_{31}N_3Cl_4OPRuS$ (M_r = 743.50 g/mol), %: C, 46.85; H, 4.20; N, 5.65; S, 4.31. Found, %: C, 46.69; H, 4.15; N, 5.62; S, 4.37. ESI-MS-

(27) Barette, W. C., Jr.; Johnson, H. W., Jr.; Sawyer, D. T. *Anal. Chem.* **1984**, *56*, 1890−1898.
(28) Guedes da Silva, M. F. C.; Pombeiro, A. J. L.; Geremia, S.; Zangrando, E.; Calligaris, M.; Zinchenko, A. V.; Kukushkin, V. Yu. *J. Chem. Soc., Dalton Trans.* **2000**, 1363−1371.
(29) Sheldrick, G. M. *SHELXS-97, Program for Crystal Structure Solution*; University of Göttingen, Germany, 1997.
(30) Sheldrick, G. M. *SHELXL-97, Program for Crystal Structure Refinement*; University of Göttingen, Germany, 1997.
(31) Johnson, C. K. Report ORNL-5138; Oak Ridge National Laboratory: Oak Ridge, TN, 1976.

(-ve), *m*/*z*: 391 $[RuCl_4(Htrz)(DMSO)]^-$; 322 $[RuCl_4(DMSO)]^-$; 244 $[RuCl_4]^-$. ESI-MS(+ve), 353 $(Ph_3PCH_2Ph)^+$. mp = 177 °C. TLC on SiO_2, R_f = 0.53 (eluent CH_2Cl_2/MeOH = 85:15). IR spectrum in KBr; selected bands, cm^{-1}: 1119 vs, 1078 vs $\upsilon(S=O)$, 426 m ν(Ru − S). UV−vis (MeOH), λ_{max}, nm (ϵ, mM^{-1} cm^{-1}): 478 (0.39), 406 (3.72), 298 (1.06). Orange crystals suitable for X-ray diffraction study were grown in an H-shaped tube by the solvent diffusion method upon reacting equimolar amounts of **A2** in ethanol and benzyltriphenylphosphonium chloride in water.

(PPN)[*trans*-RuCl$_4$(Htrz)(DMSO)] (A2b). Yellow powder. Yield: 0.17 g, 81% based on Ru. Anal. Calcd for $C_{40}H_{39}N_4Cl_4OP_2RuS$ (M_r = 928.66 g/mol), %: C, 51.73; H, 4.23; N, 6.03; S, 3.45. Found, %: C, 51.93; H, 4.03; N, 5.90; S, 3.49. ESI-MS(-ve), *m*/*z*: 391 $[RuCl_4(Htrz)(DMSO)]^-$; 322 $[RuCl_4(DMSO)]^-$; 244 $[RuCl_4]^-$. ESI-MS(+ve), 538 $(PPN)^+$. mp = 202 °C. TLC on SiO_2, R_f = 0.50 (eluent CH_2Cl_2/MeOH = 85:15). IR spectrum in KBr, selected bands, cm^{-1}: 1119 vs, 1078 vs $\upsilon(S=O)$, 428 m ν(Ru − S). UV−vis (MeOH), λ_{max}, nm (ϵ, mM^{-1} cm^{-1}): 478 (0.42), 406 (3.97), 300 (1.13). Yellow crystals suitable for X-ray diffraction study were grown in an H-shaped tube by the solvent diffusion method upon reacting equimolar amounts of **A2** in ethanol and (PPN)Cl in water.

(Ph_3PCH_2Ph)[*trans*-RuCl$_4$(Hind)(DMSO)] (A3a). Yield: 0.14 g, 79% of orange-yellow powder based on Ru. Anal. Calcd for $C_{34}H_{34}N_2Cl_4OPRuS$ (M_r = 792.57 g/mol), %: C, 51.52; H, 4.32; N, 3.53; S, 4.05. Found, %: C, 51.49; H, 4.12; N, 3.51; S, 4.02. ESI-MS(-ve), *m*/*z*: 440 $[RuCl_4(Hind)(DMSO)]^-$; 322 $[RuCl_4(DMSO)]^-$; 244 $[RuCl_4]^-$. ESI-MS(+ve), 353 $[Ph_3PCH_2Ph]^+$. mp = 190 °C. TLC on SiO_2, R_f = 0.55 (eluent CH_2Cl_2/MeOH = 85:15). IR spectrum in KBr; selected bands, cm^{-1}: 1112 vs, 1077 vs $\upsilon(S=O)$, 423 ν(Ru − S). UV−vis (MeOH), λ_{max}, nm (ϵ, mM^{-1} cm^{-1}): 476 (0.51), 406 (3.92), < 300 (absorption of benzene ring).

[(Hind)$_2$H][*trans*-RuCl$_4$(Hind)$_2$] (B3a). Na[*trans*-$RuCl_4(HInd)_2$] (0.30 g, 0.6 mmol) in water (260 mL) was added to an aqueous solution (260 mL) containing indazole (0.19 g, 1.6 mmol) and 0.2 M HCl (8 mL). The reaction mixture was filtered off, and left to stand for 48 h at 4 °C. The brown-red plates were separated by filtration, washed with water, and dried at room temperature in vacuo. Yield: 0.25 g, 58%. Anal. Calcd. for $C_{28}H_{25}N_8Cl_4Ru$ (M_r = 716.42 g/mol), %: C, 46.94; H, 3.52; N, 15.64. Found: C, 46.54; H, 3.36; N, 15.45. ESI-MS(-ve), *m*/*z*: 480 $[RuCl_4(Hind)_2]^-$; 244 $[RuCl_4]^-$. ESI-MS(+ve): 119 $[Hind]^+$. mp = 170 °C (dec). TLC on SiO_2, R_f = 0.58 (eluent CH_2Cl_2/MeOH = 50:50). IR spectrum in KBr; selected bands, cm^{-1}: 1628, 1357, 744. UV−vis (MeOH), λ_{max}, nm (ϵ, mM^{-1} cm^{-1}): 435 (0.68), 370 (4.30). Single crystals suitable for X-ray diffraction study were selected directly from the isolated product.

Results and Discussion

Synthesis and Characterization of the Complexes. Complexes **A** were synthesized by reaction of $[(DMSO)_2H]$-[*trans*-$RuCl_4(DMSO)_2$] with an excess of the corresponding azole heterocycle. The corresponding (Ph_3PCH_2Ph)- or (PPN)-complex salts were obtained by metathesis of (HL)-[*trans*-$RuCl_4L(DMSO)$] and (Ph_3PCH_2Ph)Cl or (PPN)Cl. Complexes **B** were prepared starting from an HCl-acidic solution of $RuCl_3$ and an excess of azole ligand.[38]

Their electronic absorption spectra in water are similar. One main band with an absorption maximum in the 396−348 nm range, a shoulder at 462−396, and a third absorption at 293−233 in **A1**, **A2**, **B1**, and **B2** are observed (Table 1). In the spectra of **A3** and **B3b** an intense absorption band of the condensed benzene ring prevented the resolution of the latter band. Replacement of the strong π-acceptor DMSO by an azole ligand shifts the absorption maximum to shorter wavelengths. The azole ligands follow the same tendency, where the absorption maximum for the more electron donating and basic imidazole, pK_a (H_2im^+) = 7.00,[39] is blue shifted compared to 1,2,4-triazole, pK_a (H_2trz^+) = 2.55,[40] or indazole, pK_a (H_2ind^+) = 1.25.[41]

Table 1. UV-vis Absorption Bands [Wavelength and Molar Absorptivity (in brackets)] for Complexes **A** and **B** in Water at Room Temperature

complex	λ_{max} (nm)	ϵ (mM^{-1} cm^{-1})[a]	
(H_2im)[*trans*-$RuCl_4$(Him)(DMSO)] **A1**	452 (0.49)	390 (3.64)	288
(H_2trz)[*trans*-$RuCl_4$(Htrz)(DMSO)] **A2**	462 (0.45)	396 (3.76)	293
(H_2ind)[*trans*-$RuCl_4$(Hind)(DMSO)] **A3**	462 (0.65)	396 (4.33)	
(H_2im)[*trans*-$RuCl_4(Him)_2$] **B1**	396 (0.50)	348 (3.12)	233
(H_2trz)[*trans*-$RuCl_4(Htrz)_2$] **B2**	418 (0.37)	362 (2.75)	235
Na[*trans*-$RuCl_4(Hind)_2$] **B3b**	422 (1.24)	364 (4.37)	

[a] An intense UV absorption band prevented the accurate determination of the molar absorptivity for the shorter wavelength band, as well as the resolution of this band for complexes **A3** and **B3b**.

Table 2. Crystallographic Data for **A2a**, **A2b**, **A3**, and **B3a**

	A2a	**A2b**	**A3**	**B3a**
chemical formula	$C_{29}H_{31}N_3Cl_4OPRuS$	$C_{40}H_{39}N_4Cl_4OP_2RuS$	$C_{16}H_{19}N_4Cl_4ORuS$	$C_{28}H_{25}N_8Cl_4Ru$
formula weight	743.50	928.66	558.28	716.42
T, K	120	120	120	120
space group	$P\bar{1}$	$P2_1/c$	$P2_1/n$	$P\bar{1}$
a/Å	9.599(2)	17.029(3)	10.619(2)	6.602(1)
b/Å	12.680(3)	16.428(3)	8.691(2)	9.962(2)
c/Å	14.476(3)	14.653(3)	22.667(5)	11.671(2)
α/deg	112.15(3)			92.78(3)
β/deg	109.16(3)	103.32(3)	103.00(3)	102.57(3)
γ/deg	90.90(3)			104.75(3)
V/Å^3	1521.8(6)	3989.0(14)	2038.3(8)	720.1(2)
Z	2	4	4	1
λ/Å	0.71073	0.71073	0.71073	0.71073
ρ_{calcd}/g cm^{-3}	1.622	1.546	1.819	1.652
μ_{calcd}/cm^{-1}	10.17	8.32	14.11	9.51
*R*1[a]	0.0304	0.0261	0.0296	0.0355
*wR*2[b]	0.0780	0.0705	0.0709	0.0817

[a] $R1 = \sum||F_o| - |F_c||/\sum|F_o|$. [b] $wR2 = [\sum w|F_o^2| - |F_c^2|)^2/\sum w|F_o^2|^2]^{1/2}$.

(32) *International Tables for X-ray Crystallography*; Kluwer Academic Press: Dordrecht, The Netherlands, 1992; Vol. C, Tables 4.2.6.8 and 6.1.1.4.

(33) Mestroni, G.; Alessio, E.; Sava, G. Intl. Patent PCT C07F 15/00, WO98/00431, 1998.

(34) (a) Alessio, E.; Balducci, G.; Calligaris, M.; Costa, G.; Attia, W. M.; Mestroni, G. *Inorg. Chem.* **1991**, *30*, 609−618. (b) Jaswal, J. S.; Rettig, S. J.; James, B. R. *Can. J. Chem.* **1990**, *68*, 1808−1817.

(35) Keppler, B. K.; Rupp, W.; Juhl, U. M.; Endres, H.; Niebl, R.; Balzer, W. *Inorg. Chem.* **1987**, *26*, 4366−4370.

(36) Lipponer, K. G.; Vogel, E.; Keppler, B. K. *Met.-Based Drugs* **1996**, *3*, 243−260.

(37) Peti, W.; Pieper, T.; Sommer, M.; Keppler, B. K.; Giester, G. *Eur. J. Inorg. Chem.* **1999**, 1551−1555.

(38) Kralik, F.; Vrestal, J. *Collect. Czech. Chem. Commun.* **1961**, *26*, 1298−1304.

(39) Reedijk, J. Heterocyclic Nitrogen-Donor Ligands. In *Comprehensive Coordination Chemistry*; Wilkinson, G.; Gillard, R. D.; McCleverty, J. A., Eds.; Pergamon Press: Elmsford, NY, 1987; Vol. 2, pp 73−98.

(40) Potts, K. T. *Chem. Rev.* **1961**, *61*, 87−127.

Table 3. Bond Lengths (Å) and Angles (deg) for **A2a**, **A2b**, **A3**, and **B3b**

Atom1−Atom2	A2a	A2b	A3	B3a
Ru1−N4	2.1207(17)	2.1042(12)		
Ru1−N1			2.0901(13)	2.062(3)
Ru1−S1	2.2730(8)	2.2691(6)	2.2924(7)	
Ru1−Cl1	2.3373(9)	2.3705(5)	2.3497(7)	2.3602(11)
Ru1−Cl2	2.3449(12)	2.3462(5)	2.3964(9)	2.3616(10)
Ru1−Cl3	2.3730(9)	2.3421(5)	2.3460(9)	
Ru1−Cl4	2.3613(12)	2.3603(5)	2.3571(7)	
S1−O1	1.4742(16)	1.4741(10)	1.4951(12)	

Atom1−Atom2−Atom3	A2a	A2b	A3	B3a
N4−Ru1−S1	178.34(4)	176.65(3)		
N1−Ru1−S1			175.87(3)	
N1#−Ru1−N1				180.00
N4−Ru1−Cl1	89.29(5)	91.59(4)		
N1−Ru1−Cl1			88.12(3)	88.27(8)
N4−Ru1−Cl2	86.82(5)	87.57(4)		
S1−Ru1−Cl1	90.61(3)	89.89(2)	95.964(13)	
Ru1−S1−O1	118.88(7)	117.69(4)	115.09(5)	

Crystal Structures. Crystallographic data for **A2a**, **A2b**, **A3**, and **B3a** are summarized in Table 2, and selected bond lengths and angles are presented in Table 3.

The solid-state structures of **A2a** and **A2b** feature an S-bonded DMSO ligand trans to the N-donor atom of Htrz (Figures 3 and 4). To our knowledge these are the first ruthenium complexes containing one triazole ligand to be crystallographically characterized. From isotropic displacement parameters it was impossible to distinguish between carbon and nitrogen atoms in the heterocyclic ring of **A2a**. Moreover, the distribution of electron density over the triazole ring does not allow the localization of double bonds. All ring bond lengths are essentially the same. Three different models (coordination via N2, coordination via N2 with rotational (180°) disorder, or coordination via N4) were refined but no model could be favored over the two others. However, analysis of the crystal structure of **A2a** showed the presence of interanion contacts (Figure 3) which can be described as hydrogen bridges of the H−N1−N2 parts of the triazole rings with the following parameters: N1−H = 0.86 Å, H···N2′ = 2.656 Å, N1···N2′ = 3.262 Å, ∠N1HN2′ = 128.6°. In addition, the interplanar separation between the interacting triazole rings is 0.89 Å. Similar but stronger interactions have been observed for $Cd(NCS)_2(Htrz)_2$.[42] Hence, coordination of triazole via N4 is proposed, and the same coordination mode has been revealed in **A2b**. In contrast, however, in this complex a remarkable difference in ring bond lengths of triazole was found. In particular the N2−C3 bond at 1.3176(18) Å is about 5σ shorter than the same bond in **A2a** at 1.335(3) Å. On the other hand, the bond angles in the triazole ring, both in **A2a** and **A2b**, are very similar, providing an additional piece of evidence for the same coordination mode of Htrz in **A2a** and **A2b**. The Ru1−S1 bond distances are 2.2730(8) and 2.2691(6) Å, and the S1−O1 bond lengths are 1.4742(16) and 1.4741(10) Å

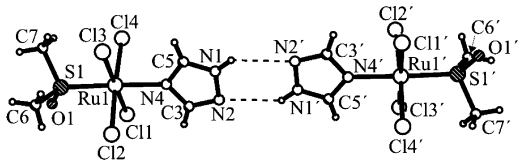

Figure 3. Structure of [*trans*-$RuCl_4$(Htrz)(DMSO)]$^-$ in **A2a**.

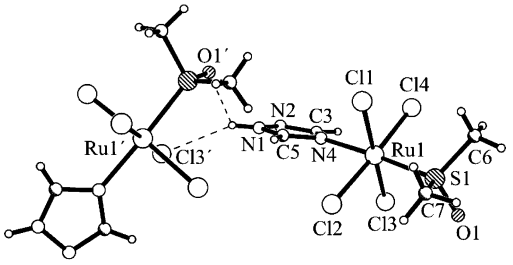

Figure 4. Structure of [*trans*-$RuCl_4$(Htrz)(DMSO)]$^-$ in **A2b**.

in **A2a** and **A2b**, correspondingly. This latter bond is markedly shorter than the one in free DMSO [1.492(1) Å][43] indicating greater S−O double bond character for the S-bonded molecule. Both Ru1−S1 and S1−O1 are slightly shorter than those found in Na[*trans*-$RuCl_4(NH_3)$(DMSO)] [2.2797(7) and 1.479(3) Å, respectively] and significantly shorter than those in Na[*trans*-$RuCl_4$(Him)(DMSO)] [2.2956(6) and 1.487(2) Å].[17] The N1−H group of the triazole ring appears to form a bifurcated hydrogen bond involving O1′ (x, 0.5 − y, z − 0.5) as well as Cl3′ (x, 0.5 − y, z − 0.5) (O1′···H 2.37(1) Å, H−N1 0.90(1) Å, and O1′···H−N1 112.0(1)°; Cl3′···H 2.57(1) Å, H−N1 0.90(1) Å, Cl3′···H−N1 149.1(1)°) (Figure 4). Bond lengths and angles in the $(Ph_3PCH_2Ph)^+$ and $(PPN)^+$ cations are similiar to those found elsewhere.[44,45]

The proposed binding mode agrees well with the higher basicity of N4 in comparison to that of N2.[46] In $[Mn^{II}(Htrz)(H_2O)_4(SO_4)]$,[47] $[Cd(Htrz)_2(NCS)_2]$,[42] and $[Fe(bpy)(Htrz)Cl_3]$[48] coordination via N4 to the metal ion has been established by X-ray crystallography. The same coordination mode of triazole was proposed for Zn(II) in human carbonic anhydrase,[48,49] as a result of hydrogen bonding.

The ruthenium(III) atom in **A3** has the expected distorted octahedral geometry (Figure 5), with four chloride ligands in the equatorial positions and a DMSO molecule bound through its sulfur atom *trans* to the indazole ligand in axial positions. The average value of the Ru−Cl bond lengths [2.362(12) Å] is comparable with those found in Na[*trans*-$[RuCl_4$(Him)(DMSO)]·H_2O·Me_2CO[17] and $[(DMSO)_2H][RuCl_4(DMSO)_2]$[34] [2.342(7) and 2.348(4) Å, respectively]. The

(41) Catalán, J.; Claramunt, R. M.; Elguero, J.; Laynez, J.; Menéndez, M.; Anvia, F.; Quian, J. H.; Taagepera, M.; Taft, R. W. *J. Am. Chem. Soc.* **1988**, *110*, 4105−4111.
(42) Haasnoot, J. G.; De Keyzer, G. C. M.; Verschoor, G. C. *Acta Crystallogr.* **1983**, *C39*, 1207−1209.
(43) Calligaris, M.; Carugo, O. *Coord. Chem. Rev.* **1996**, *153*, 83−154.
(44) Cifuentes, M. P.; Waterman, S. M.; Humphrey, M. G.; Heath, G. A.; Skelton, B. H.; White, A. H.; Seneka Perera, M. P.; Williams, M. L. *J. Organomet. Chem.* **1998**, *565*, 193−200.
(45) Bartczak, T. J.; Wolowiec, S.; Latos-Grazynski, L. *Inorg. Chim. Acta* **1998**, *277*, 242−246.
(46) Meot-Ner, M.; Liebman, J. F.; Del Bene, J. E. *J. Org. Chem.* **1986**, *51*, 1105−1110.
(47) Gorter, S.; Engelfriet, D. W. *Acta Crystallogr.* **1981**, *B37*, 1214−1218.
(48) Haasnoot, J. G. *Coord. Chem. Rev.* **2000**, *200*−*202*, 131−185.
(49) Mangani, S.; Liljas, A. *J. Mol. Biol.* **1993**, 232, 9−14.

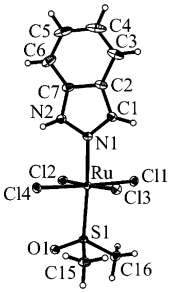

Figure 5. Structure of [*trans*-$RuCl_4$(Hind)(DMSO)]$^-$ in **A3**.

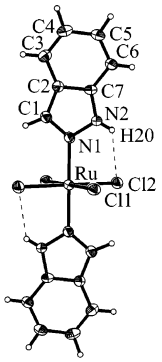

Figure 6. Structure of [*trans*-$RuCl_4(Hind)_2$]$^-$ in **B3a**.

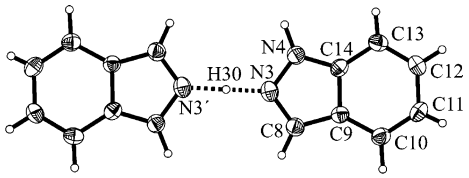

Figure 7. Structure of $(Hind)_2H^+$ in **B3a**.

Ru−N1 bond [2.0901(13) Å] is significantly longer than those in (Ph_4P)[*trans*-$RuCl_4(Hind)_2$][37] [2.0517(21) and 2.0711(22) Å] and 8.5 σ longer than that in $[(Hind)_2H]$[*trans*-$RuCl_4(Hind)_2$] (see below) [2.062(3) Å], which is expected taking into account the stronger *trans*-influence of the S atom of DMSO when compared to the N atom of the azole ligand.[17] However, the Ru−S1 bond (sulfur being trans to the indazole nitrogen) [2.2924(7) Å] is markedly shorter than that found in $[(DMSO)_2H][RuCl_4(DMSO)_2]$ [2.348(1) Å] with mutually *trans* dimethyl sulfoxide ligands.[34] Thus, replacement of one of the DMSOs by an indazole ligand results in a shortening of the other Ru−DM*S*O bond due to a diminished π-back-bonding competition between the two *trans*-ligands or decreased σ-directed trans influence of nitrogen ligand. The S═O bond length of 1.4951(12) Å is slightly longer than that of free DMSO [1.492(1) Å][43] indicating a greater S−O single bond character for the S-bonded molecule.

The crystal structure of **B3a** consists of the complex anions [*trans*-$RuCl_4(Hind)_2$]$^-$ (Figure 6) and the unusual $[(Hind)\cdots H\cdots(Hind)]^+$ cations (Figure 7). It displays a distorted octahedral coordination with four chloride ions in the equatorial plane and two indazole ligands in axial positions. The structure of the anion is stabilized by two symmetry related intramolecular hydrogen bonds of the type N−H···Cl (N2−H20 0.76 Å, H20···Cl2 2.68 Å, N2···Cl2 3.15 Å, ∠N2H20Cl2 121.9°). In contrast to (Ph_4P)[*trans*-$RuCl_4(Hind)_2$][37] the ruthenium atom in **B3a** lies at a center of

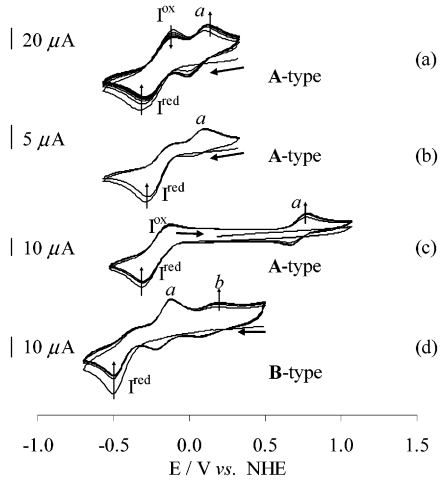

Figure 8. Multiple scan cyclic voltammograms of 5 mM (H_2im)[*trans*-$RuCl_4$(Him)(DMSO)] **A1** in DMF (a and b) or DMSO (c) and (H_2ind)-[*trans*-$RuCl_4(Hind)_2$] **B3** (d) in DMF, with 0.15 M [nBu$_4$N][BF_4], at a carbon disk working electrode and at a scan rate of 2 (a), 0.2 (b), or 1 (c and d) V s^{-1}.

symmetry. The Ru−N1 bond distance [2.062(3) Å] is intermediate between those found in (Ph_4P)[*trans*-$RuCl_4(Hind)_2$] [2.0517(21) and 2.0711(22) Å]. The Ru−Cl bond distances [2.3602(11) and 2.3616(10) Å] are comparable to those in the ruthenium tetraphenylphosphonium salt [average 2.3639(8) Å].[37] Both indazole ligands lie in one plane in contrast to what was found in (Ph_4P)[*trans*-$RuCl_4(Hind)_2$] where they were significantly twisted. The plane through both indazole ligands crosses the equatorial plane between Cl1 and Cl2, the torsion angle Cl1−Ru−N1−N2 and the angle Cl1−Ru−Cl2 being 63.5(2)° and 90.33(4)°, respectively. The distribution of electron density over the *trans* indazole ligands in both complexes is also similar.

Very strong H-bond(s) between the two indazole units of the cation were found. This interaction can be classified as a homonuclear centered H-bond of the type A in accordance with Speakman classification,[50] with the proton located in a center of symmetry. The interatomic separation N3···N3′ [2.664 Å] is significantly shorter than the van der Waals radius of the nitrogen atom [3.10 Å].[50] Crystallographic data on the hydrogen-bonded cations are relatively scarce.[51]

Electrochemical Studies. Cathodic Behavior in Aprotic Media. The cyclic voltammograms of 0.15 M [nBu$_4$N][BF_4]/DMF or DMSO solutions of the complexes (HL)[*trans*-$RuCl_4L(DMSO)$] (**A**) and (HL)[*trans*-$RuCl_4L_2$] (**B**) [L = imidazole (Him), 1,2,4-triazole (Htrz) or indazole (Hind)], at a glassy carbon working electrode and at a scan rate of 0.2 V s^{-1} display (Figures 8−10) one quasireversible (for **A**) or irreversible (for **B**) single-electron (as confirmed by cathodic controlled potential electrolyses (CPE) of **A1** and **B3**) reduction wave, I^{red}, which is assigned to the $Ru^{III}\rightarrow Ru^{II}$ process. The reduction potentials (Table 4) for compounds **A** ($E_{1/2}^{red} = -0.04$ to -0.23 V) are considerably higher than those for **B** ($E_{p/2}^{red} = -0.41$ to -0.74 V) which agrees with the stronger net electron-acceptor character of the S-

(50) Emsley, J. *Chem. Soc. Rev.* **1980**, *9*, 91−124.
(51) James, B. R.; Morris, R. H.; Einstein, F. W. B.; Willis, A. *J. Chem. Soc. Chem. Commun.* **1980**, 31−32.

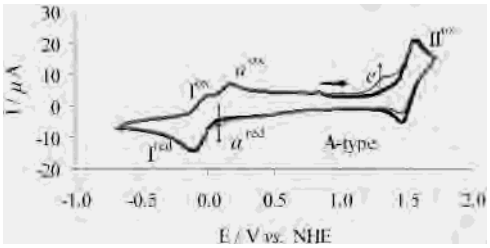

Figure 9. Cyclic voltammogram of 5 mM (H_2trz)[*trans*-$RuCl_4$(Htrz)-(DMSO)] **A2**, in DMF with 0.15 M [*n*Bu_4N][BF_4], at a carbon disk working electrode and at a scan rate of 0.2 V s^{-1}, showing two consecutive scan cycles [first (black line) and second (gray line) scan].

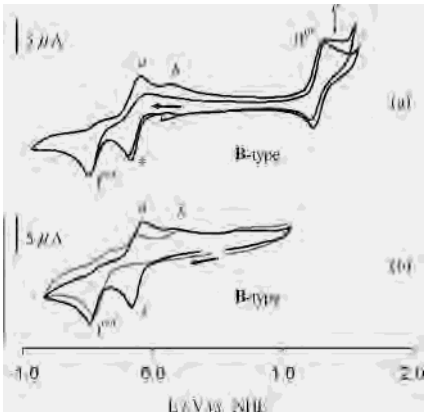

Figure 10. Cyclic voltammograms of a 5 mM (H_2ind)[*trans*-$RuCl_4$(Hind)$_2$] **B3** solution in DMF with 0.15 M [*n*Bu_4N][BF_4] at a scan rate of 0.2 V s^{-1} and at a platinum disk (black line) or glassy carbon (gray line) working electrode with scan reversal following wave * or the reduction wave I^{red} (a), or showing the effect of replacing the latter by the former electrode (b).

coordinated DMSO ligand as compared with the azole ones (see below) and with the more effective σ-donor ability of the latter ligands. In addition, in both series of compounds, the reduction potentials of the Htrz complexes are less cathodic than those of the Him ones, in accord with the relative electron-donor character of the N-ligands.

By replacing the vitreous carbon disk by a platinum disk working electrode, the cathodic pattern for both types (**A** and **B**) of complexes is as described above, apart from the detection of an additional irreversible reduction wave [at potential values of $E_p^{red} = -0.52$ V (**A1** and **B1**), -0.20 V (**A2** and **B2**), -0.14 V (**A3** and **B3**), or -0.15 V (**B3a**, wave * in Figure 10)] which is due to the protic reduction of the azolium counterions H_2im^+, H_2trz^+, H_2ind^+, or $(Hind)_2H^+$, respectively. The values for triazolium $(H_2trz)^+$ and imidazolium $(H_2im)^+$ are in agreement with those found in the literature.[13,52]

The $E_{1/2}^{red}$ values for complexes **A** and **B** are in good agreement with those expected on the basis of the general equation (eq 1) proposed by Lever, by using the known values of S_M and I_M (0.97 and 0.04, respectively)[19] for the Ru^{III}/Ru^{II} redox couple and the E_L values for the various ligands [$E_L(Cl^-) = -0.24$,[19] E_L(DMSO) = 0.57,[28] E_L(Him) = 0.12,[19] and E_L(Htrz) = 0.18[19]] (Table 4). Moreover, the application of eq 1, considering the experimental values of

Table 4. Cyclic Voltammetric Data for (HL)[*trans*-$RuCl_4$L(DMSO)] (**A**) and (HL)[*trans*-$RuCl_4L_2$] (**B**) [L = Him (**A1** and **B1**), Htrz (**A2** and **B2**), or Hind (**A3** and **B3**)] and Estimated Redox Potential Values

	Experimental[a]					Calculated[b]		
complex	E^{red}/I^{red}	E^{ox}/II^{ox}	E^{ox}/a^c	E^{ox}/b^c	E^{ox}/a'^c	E/I^{red}	E/a	E/b
A1[d]	−0.22	1.45	0.02			−0.22	0.04	
	(−0.23)		(0.66)				(0.57)	
A2	−0.06	1.51	0.13			−0.16	0.10	
	(−0.09)		(0.75)				(0.63)	
A3	−0.04	1.55*	0.17					
	(−0.10)		(0.78)					
B1	−0.72*	0.96	−0.49	−0.15	1.29	−0.66	−0.39	−0.12
	(−0.74)*	(0.99)						
B2	−0.48*	1.18	−0.21	0.03	1.43	−0.54	−0.28	0.00
	(−0.44)*	(1.19)						
B3[e]	−0.43*	1.27	−0.15	0.16	1.55			
	(−0.41)*	(1.27)						

[a] Potentials in V ± 0.02 vs NHE measured at a scan rate of 0.2 V s^{-1}, in 0.15 M [*n*Bu_4N][BF_4]/DMF (or DMSO, in brackets). $E_{1/2}$ values are given for the reversible waves, whereas for the irreversible ones, the $E_{p/2}$ values are indicated by an asterisk. [b] Potentials in V vs NHE estimated from eq 1 with S_M and I_M values of 0.97 and 0.04, respectively, and known E_L for the ligands (see text). Values in brackets refer to the DMSO derivative. [c] Oxidation waves for the complexes formed upon the first [(*a*) (Ru^{II}/Ru^{III}) and (*a*′) (Ru^{III}/Ru^{IV})] and the second [(*b*) (Ru^{II}/Ru^{III})] chloride replacement by solvent molecules detected upon scan reversal after the formation of wave I^{red} (see text, Figures 8−10, and Schemes 1 and 2). [d] Wave *b* and the additional waves *c* and *d* of the complexes (see text) formed by further chloride replacement by solvent are observed after CPE, at E^{ox} values of 0.31, 0.67, and 0.97 V, respectively; the corresponding estimated values are 0.30, 0.56, and 0.83 V vs NHE. [e] Waves *c* and *d* of the complexes (see text) formed by further chloride replacement by solvent are observed after CPE, at E^{ox} values of 0.43 and 0.62 V, respectively; the corresponding estimated values are 0.35 and 0.64 V vs NHE.

the oxidation potentials of [*trans*-$RuCl_4$(Hind)(DMSO)]$^-$ (**A3**) and [*trans*-$RuCl_4(Hind)_2]^-$ (**B3**) in DMF and DMSO solutions, the known values of E_L ligand parameters and of S_M and I_M (see above), enabled the estimate of the yet unknown E_L ligand parameter for indazole as an average of four values (two measured in DMF and further two in DMSO) obtained in this work: E_L(Hind) = 0.26 V vs NHE. It is higher than those of triazole and imidazole, indicating that indazole is a weaker net electron-donor than the other ligands.

Upon potential scan-reversal following the formation of wave I^{red} [but not of wave * (Figure 10a)], one (wave *a*, for **A**, Figures 8a−c and 9) or two (waves *a* and *b*, for **B**, Figures 8d and 10) quasireversible oxidation waves are detected, being due to the oxidation of products formed in the cathodic processes. CPE at the cathodic wave I^{red} generates several species as indicated by monitoring the electrolysis by cyclic voltammetry (CV) (apart from waves *a* and *b*, two other waves, *c* and *d*, are detected at higher potentials, Figure S1 in the Supporting Information). Attempts to isolate these products failed, but on the basis of the agreement between the measured values of the oxidation potentials of these waves from each complex (0.02, 0.31, 0.67, and 0.96 V from **A1** and −0.15, 0.16, 0.43, and 0.62 V from **B3**) and the predicted ones [0.04, 0.30, 0.56, and 0.83 V and −0.14, 0.12, 0.35, and 0.64 V, respectively, by applying Lever's equation (eq 1) and the known E_L values (see above) for chloride, DMSO and Him, as well as for DMF (0.03 V)[53]] we propose the following formulations, derived from chloride ligand dis-

(52) Serli, B.; Zangrando, E.; Iengo, E.; Mestroni, G.; Yellowlees, L.; Alessio, E. *Inorg. Chem.* **2002**, *41*, 4033−4043.

(53) http://www.chem.yorku.ca/profs/lever (homepage of A. B. P. Lever).

Scheme 1. Anodic and Proposed Cathodic Processes of Complexes **A**. L′ = DMF or DMSO

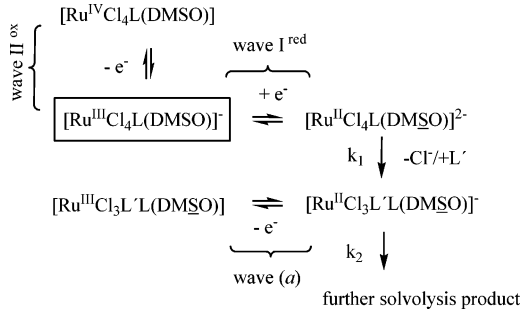

Scheme 2. Anodic and Proposed Cathodic Processes of Complexes **B**. L′ = DMF

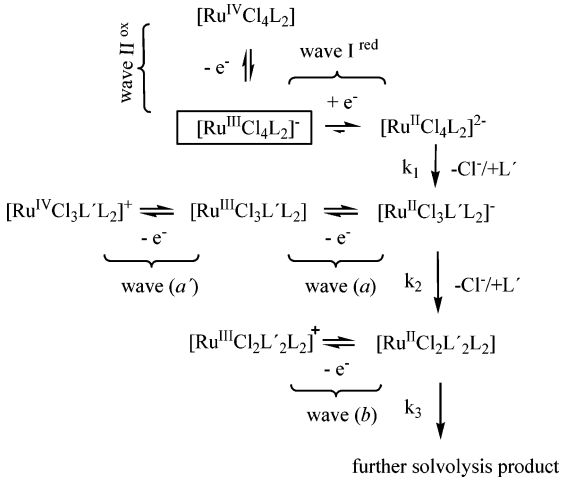

placement at Ru^{II} by solvent (Schemes 1 and 2, depending on the starting complex **A** or **B**): (*a*), $[Ru^{II}Cl_3(DMF)L(DMSO)]^-$ or $[Ru^{II}Cl_3(DMF)L_2]^-$; (*b*), $[Ru^{II}Cl_2(DMF)_2L(DMSO)]$ or $[Ru^{II}Cl_2(DMF)_2L_2]$; (*c*), $[Ru^{II}Cl(DMF)_3L(DMSO)]^+$ or $[Ru^{II}Cl(DMF)_3L_2]^+$; and (*d*), $[Ru^{II}(DMF)_4L(DMSO)]^{2+}$ or $[Ru^{II}(DMF)_4L_2]^{2+}$. In the time-scale of electrolysis and for both complexes, the formation of species (*c*) appears to be dominant as suggested by the predominance of the current intensity of its wave as compared with the others. Furthermore, for complexes **B**, the quasireversible second oxidation (Ru^{III}/Ru^{IV}) of $[RuCl_3(DMF)L_2]^-$ (wave *a*′), formed in the cathodic process upon $Ru^{III} \rightarrow Ru^{II}$ reduction (wave I^{red}), was also observed by running a simple CV (Table 4). For complexes **A** the onset of the solvent−electrolyte discharge potential prevented the detection of the corresponding $Ru^{III} \rightarrow Ru^{IV}$ oxidation waves.

A further evidence for chloride loss upon reduction of the complexes under study is the oxidation wave (*e*) (Figures 9 and 10a) detected in the subsequent anodic scan upon formation of wave I^{red}, at potential values ($E_p = 1.30 - 1.40$ V) identical to those measured for the oxidation of Cl^- in solutions of $(Ph_3PCH_2Ph)Cl$, (PPN)Cl, or $(Me_4N)Cl$ under the same experimental conditions. The cathodically induced chloride loss, with the concomitant formation of the above products, is a well documented type of reaction.[28,54−56] In addition, it is also known that halide is relatively inert to substitution in the coordination sphere of ruthenium(III),[52,57,58] but as a strong σ-donor and a potential π-donor it is labile at Ru(II), itself a good π-donor where all t_{2g} orbitals are filled.[59]

This is also consistent with the known promotion of hydrolysis of chloride ligands for compound **A1** upon chemical reduction by biological reductants (e.g., ascorbic acid), in aqueous physiological conditions, as shown by UV−vis and ^1H NMR studies (but not by electrochemical methods).[10,60,61]

The high-scan-rate-limiting behaviors of Schemes 1 and 2 should correspond to the quasireversible single-electron reduction of **A** or **B** since there would be no time for appreciable dechlorination. For complexes **A** cyclic voltammograms at scan rates higher than 10 V s^{-1} reveal a $^{I}i_p^{ox}/{}^{I}i_p^{red}$ ratio equal to 1, but such a limiting behavior is not yet achieved for complexes **B** up to 40 V s^{-1}. Upon decreasing the scan rate, there occurs an increasing conversion of **A** or **B** into the solvolysis products (Figures 8a and b), and multiple scans at a given scan rate result in an increase of wave *a* (Figures 8a and c) or *b* (Figure 8d) with time. No significant variation of the above behaviors was detected upon changing the concentration of the complexes, thus indicating the involvement of first-order chemical steps.

Kinetic Investigation of the Cathodically Induced Replacement of Chloride. The mechanisms of Schemes 1 and 2 were investigated in detail by digital simulation (program ESP)[62] of the cyclic voltammograms in the available range of scan rates (0.01−30 V s^{-1}). A good fit was obtained (Figures 11 and 12) for the degree of reversibility of the cathodic wave I^{red}, i.e. $^{I}i_p^{ox}/{}^{I}i_p^{red}$, and the extent of formation of the chloride displacement product, i.e. the normalized peak-current of wave (*a*), $^{a}i_p^{ox}/{}^{I}i_p^{red}$ (ρ) (Figure 12), and wave (*b*), $^{b}i_p^{ox}/{}^{I}i_p^{red}$ (ρ') (Figure 12d) as a function of scan rate. The lowering of the first parameter relative to the unit reflects the extent of the chemical reaction following the electron transfer (chloride replacement by solvent), whereas ρ and ρ' are determined by the relative amount of the formed corresponding solvent complex. The optimized values of the homogeneous rate constants for the first (k_1), second (k_2), and third (k_3, only for **B**) replacement of chloride by DMF are quoted in Table 5. The effect of the rate constant on the reversibility of the reduction wave and on the ρ parameter is clearly observed in Figure 12a−c: a decrease in the former results in (i) an increase of the reversibility

(54) Salih, T. A.; Duarte, M. T.; Fraústo da Silva, J. J. R.; Galvão, A. M.; Guedes da Silva, M. F. C.; Hitchcock, P. B.; Hughes, D. L.; Pickett, C. J.; Pombeiro, A. J. L.; Richards, R. L. *J. Chem. Soc., Dalton Trans.* **1993**, 3015−3023.
(55) Costa, G.; Balducci, G.; Alessio, E.; Tavagnacco, C.; Mestroni, G. *J. Electroanal. Chem.* **1990**, *296*, 57−76.
(56) Duff, C. M.; Heath, G. A. *J. Chem. Soc., Dalton Trans.* **1991**, 2401−2411.
(57) Zanella, A. W.; Ford, P. C. *Inorg. Chem.* **1975**, *14*, 42−47.
(58) Coleman, G. N.; Gesler, J. W.; Shirley, F. A.; Kuempel, J. R. *Inorg. Chem.* **1973**, *12*, 1036−1038.
(59) Ford, P. C. *Coord. Chem. Rev.* **1970**, *5*, 75−99.
(60) Sava, G.; Bergamo, A.; Zorzet, S.; Gava, B.; Casarsa, C.; Cocchietto, M.; Furlani, A.; Scarcia, V.; Serli, B.; Iengo, E.; Alessio, E.; Mestroni, G. *Eur. J. Cancer* **2002**, *38*, 427−435.
(61) Iengo, E.; Mestroni, G.; Geremia, S.; Calligaris, S.; Alessio, E. *J. Chem. Soc. Dalton Trans.* **1999**, 3361−3371.
(62) Nervi, C. *Electrochemical Simulation Package, ESP, version 2.4*; Dipartimento di Chimica IFM: Torino, Italy, 1994/98; (nervi@lem.ch.unito.it).

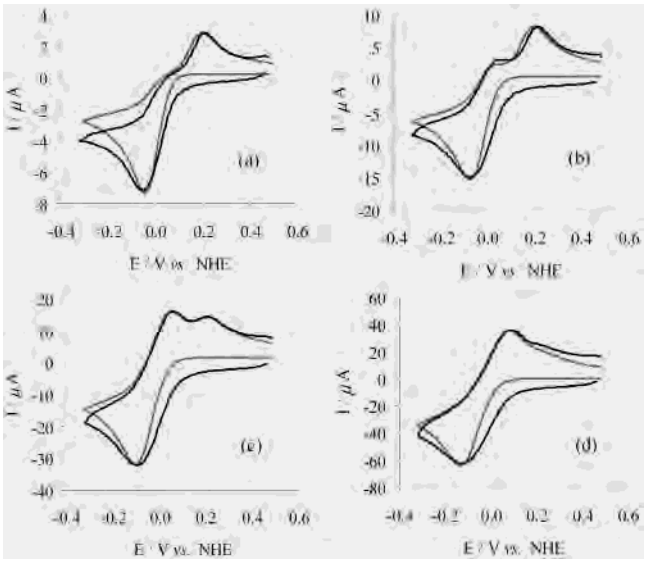

Figure 11. Experimental (10 mM, black line) and simulated cyclic voltammograms (gray line) for (H_2ind)[*trans*-$RuCl_4$(Hind)(DMSO)] **A3** in DMF with 0.15 M [$n$$Bu_4N$][$BF_4$] at a carbon working electrode and at a scan rate of 0.02 (a), 0.1 (b), 0.5 (c), and 2 (d) V s^{-1}. The simulated voltammograms were obtained by using the optimized values of the rate constants given in Table 5.

with a shift of the inflection point of the ${}^{I}i_p^{ox}/{}^{I}i_p^{red}$ curve to lower scan rates and (ii) a concomitant shift of the maximum of the ρ curve. Both rate constants increase with the net electron donor/acceptor character of the azole ligand (as expressed by E_L) and with its protic basicity (increase of pK_a of the corresponding free azolium acid H_2L^+).

The promotion of the rate of the first chloride hydrolysis by an increase of the basicity of the nitrogen heterocyclic ligand was recognized,[61] although in a qualitative way and in aqueous medium, for related chloro−Ru^{III} complexes. However, generalizations for dinuclear complexes with a bridging *N*,*N*-heterocyclic ligand[61] should be taken cautiously in view of the dependence of the rate on the oxidation states of both metals.

Although the accurate determination of the solvolysis rate constants of compounds **B** was hampered by the absence of wave I^{ox} over a wide range of potential scan rates (Figure 12d), we observed that their values are higher than the corresponding ones found for **A** and follow their general tendency. Dechlorination is thus promoted by an increase of the electron transfer from the neutral ligands to the metal with a conceivable concomitant weakening of the metal−chloride ligand bonds. However, the rate of chloride displacement decreases with the degree of substitution ($k_1 > k_2 > k_3$) (Table 5).

Anodic Behavior in Aprotic Media. The cyclic voltammograms of 0.15 M [$n$$Bu_4N$][$BF_4$]/DMF or DMSO solutions of complexes **A** and **B** present one quasireversible (irreversible in the case of **A3**) single-electron oxidation wave (wave II^{ox}, Figures 9 and 10a) at oxidation potential values of 1.45−1.55 (**A**) or 0.96−1.27 (**B**) V vs NHE (Table 4), which is assigned to the $Ru^{III}\rightarrow Ru^{IV}$ oxidation. The oxidation potential of wave II^{ox} reflects, in each set of compounds, the relative donor/acceptor abilities of the DMSO and the azole ligands as measured by E_L and shown by the plot of Figure 13, which

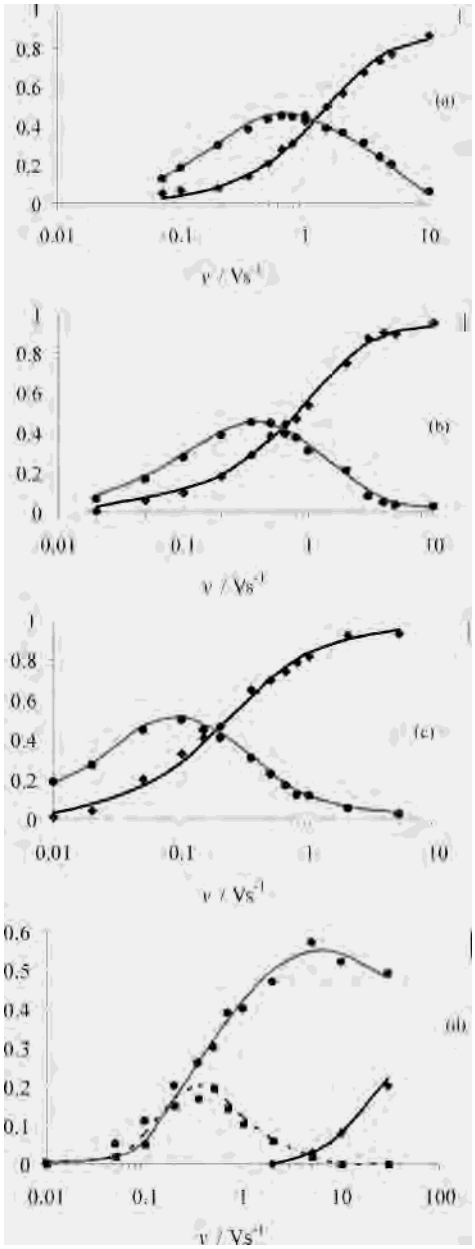

Figure 12. Experimental (symbols) and theoretical (lines) variations of the reversibility of the Ru^{III}/Ru^{II} reduction wave I, ${}^{I}i_p^{ox}/{}^{I}i_p^{red}$ (◆, black solid line), of the parameters $\rho = {}^{a}i_p^{ox}/{}^{I}i_p^{red}$ (●, gray solid line) and $\rho' = {}^{b}i_p^{ox}/{}^{I}i_p^{red}$ (■, black dashed line) as a function of scan rate (logarithmic scale) for compounds **A1** (a), **A2** (b), **A3** (c), and **B3** (d). Experimental error bars are shown at the top right corner. The theoretical lines were obtained by considering the optimized rate constant values given in Table 5.

includes also the available[56] redox potentials for the Ru^{III}/Ru^{IV} couple of the complexes $[RuX_{6-n}(RCN)_n]^{z/z-}$ (X = Cl^-, Br^- and R = Me, Ph). This relationship is expressed by eq 2 ($r = 0.98$), which allowed the estimate, for the first time, of S_M and I_M (compare with eq 1) for the $Ru^{III/IV}$ redox couple in organic solvents: $S_M = 1.03$ and $I_M = 1.68$ V vs NHE.

$$E = 1.03 \cdot \sum E_L + 1.68 \qquad (2)$$

The slope (S_M) is similar to that of the $Ru^{III/II}$ redox couple and therefore the redox potentials of the $Ru^{III/IV}$ and $Ru^{III/II}$ centers display a comparable sensitivity to a change of ligands. However, in view of the limited number of points,

Table 5. Kinetic Data[a] for (HL)[*trans*-$RuCl_4L(DMSO)$] (**A**) and (HL)[*trans*-$RuCl_4L_2$] (**B**) [L = Him (**A1** and **B1**), Htrz (**A2** and **B2**), or Hind (**A3** and **B3**)], E_L Values for the Azole Ligands (L) and pK_a Values for the Free Azolium Acids (H_2L^+)

compound	k_1/s^{-1}	k_2/s^{-1}	k_3/s^{-1}	E_L(L)	pK_a (H_2L^+)
A1	3.1 ± 0.2	0.20 ± 0.02		0.12[b]	7.00[d]
A2	1.4 ± 0.3	0.12 ± 0.03		0.18[b]	2.55[d]
A3	0.7 ± 0.2	0.03 ± 0.02		0.26[c]	1.25[d]
B1	> 200	$(5 \pm 1)\cdot 10$	0.4 ± 0.2	0.12[b]	7.00[d]
B2	$(10 \pm 5)\cdot 10$	1 ± 0.5	0.3 ± 0.1	0.18[b]	2.55[d]
B3	$(8 \pm 5)\cdot 10$	0.5 ± 0.2	0.2 ± 0.1	0.26[c]	1.25[d]

[a] The homogeneous rate constants k_1, k_2, and k_3 were determined by using the ESP simulation program (ref 62) with k_{het} of $(5 \pm 1)\cdot 10^{-3}$ cm s^{-1}. [b] From ref 19. [c] Estimated from eq 1, by using the known (ref 19) values of S_M and I_M, and E_L for the other ligands (see text). [d] From refs 39−41.

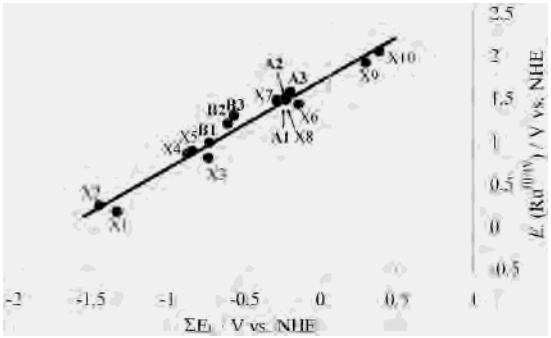

Figure 13. Plot of $E_{1/2}^{ox}$ (Ru^{III}/Ru^{IV}) against ΣE_L (in V vs NHE) for the following complexes: (HL)[*trans*-$RuCl_4L(DMSO)$] (**A**) and (HL)[*trans*-$RuCl_4L_2$] (**B**) (II^{ox}) in DMF (this work); $(Bu_4N)_2[RuX_6]$ (X = Br, **X1**; Cl, **X2**), $(Bu_4N)_2[RuX_5(RCN)]$ (X = Br, R = Ph, **X3**; Cl, Me, **X4**; Cl, Ph, **X5**), $(Bu_4N)[RuX_4(RCN)_2]$ (Br, Ph, **X6**; Cl, Me, **X7**; Cl, Ph, **X8**), $[RuX_3(RCN)_3]$ (Cl, Me, **X9**; Cl, Ph, **X10**) in CH_2Cl_2 or CH_2Cl_2/RCN (R = Me, Ph) (ref 56). $E = 1.03\cdot\Sigma E_L + 1.68$ ($r = 0.98$).

Table 6. Cyclic Voltammetric Data[a] for (HL)[*trans*-$RuCl_4L(DMSO)$] (**A**) and (HL)[*trans*-$RuCl_4L_2$] (**B**) [L = Him (**A1** and **B1**), Htrz (**A2** and **B2**), or Hind (**A3** and **B3b**[c])] in Aqueous Phosphate Buffer, pH 7

compound	$E_{1/2}^{red}/I^{red}$ [a]
A1	0.25[b]
A2	0.30
A3	0.35
B1	−0.16[b]
B2	0.00
B3b[c]	0.03

[a] Values in V ± 0.02 vs NHE. [b] Values in agreement with those given in the literature (ref 17 and 63). [c] Na[*trans*-$RuCl_4(Hind)_2$], **B3b**, was used instead of the indazolium salt, **B3**, due to the low solubility of the latter in the aqueous electrolyte solution.

further studies on a wider variety of Ru^{III}/Ru^{IV} metal complexes are required before the generality of eq 2 can be fully recognized.

Electrochemical Behavior in Aqueous Phosphate Buffer at pH 7. The cyclic voltammograms of complexes **A** and **B** in 0.2 M phosphate buffer, pH 7, at a carbon disk working electrode display one quasireversible single-electron reduction wave assigned to the $Ru^{III} \rightarrow Ru^{II}$ process, at $E_{1/2}^{red}$ potential values ranging from 0.25 to 0.35 (for **A**) or −0.16 to 0.03 (for **B**) V vs NHE (Table 6), i.e., ca. 0.4−0.6 V less cathodic than those measured in the organic solvents.

The linear relationship between the reduction potential and ΣE_L expressed by eq 3 ($r = 0.99$) was obtained from the plot of Figure 14, which includes not only our complexes **A** and **B**, but also Na[$RuCl_4$(Hpy)(DMSO)] (Hpy = pyrazole)

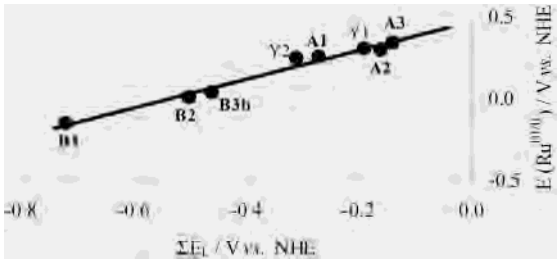

Figure 14. Plot of $E_{1/2}^{red}$ (I^{red}) for complexes (HL)[*trans*-$RuCl_4L(DMSO)$] (**A**) and (HL)[*trans*-$RuCl_4L_2$] (**B**) in aqueous phosphate buffer, pH 7, against ΣE_L (in V vs. NHE). $E = 0.88\cdot\Sigma E_L + 0.46$ ($r = 0.99$). **Y1** = Na[*trans*-$RuCl_4$(Hpy)(DMSO)] ($E_{1/2} = 0.30$ V),[17] and **Y2** = Na[*trans*-$RuCl_4$(Meim)-(DMSO)] ($E_{1/2} = 0.24$ V),[17] where E_L (Hpy) = 0.20,[19] and E_L (Meim) = 0.08 V.[19]

and Na[$RuCl_4$(Meim)(DMSO)] (Meim = *N*-methylimidazole) whose redox potentials were reported[17] by others. This expression allows estimation of, for the first time, the S_M and I_M values for the $Ru^{III/II}$ redox couple for 1− charged Ru^{III} complexes, in aqueous phosphate buffer at pH 7.

$$E = 0.88\cdot\sum E_L + 0.46 \qquad (3)$$

However, since in aqueous medium the redox potential can strongly depend on the pH of the solution,[19,63] as well as on the net charge of the complex,[19] this expression is not expected to be valid when the solution pH or the complex net charge is different from the above.

Despite the quasireversible character of the reduction wave during the CV time scale of the experiment, exhaustive cathodic CPE of complex **A1** in phosphate buffer, pH 7, results in the disappearance of the Ru^{III}/Ru^{II} wave of the starting compound, and does not reveal any new electroactive species. However, CV of a 0.2 M KNO_3 solution of complexes **A** reveals the I^{red} wave of the Ru^{III}/Ru^{II} couple and, in the subsequent anodic scan, an additional quasireversible oxidation wave (*a*) of a species formed upon reduction, at a potential that is 0.12 V higher than that of the starting Ru^{III}/Ru^{II} couple. The similarity of the latter behavior with that (see above) in DMF or DMSO and earlier NMR studies[60,61] on the hydrolysis of **A1** upon reduction in aqueous medium with biological reductants, suggest ligand chloride loss with replacement by the solvent (water) as the initial chemical reaction upon reduction.

Conclusions

Lever's general equation[19] was shown to predict well the reduction potentials of our ruthenium(III) anticancer drugs with the general formulas [*trans*-$RuCl_4L(DMSO)]^-$ and [*trans*-$RuCl_4L_2]^-$ in organic media, and a particular form of that expression was proposed to be applied to (1−) negatively charged Ru^{III} complexes in aqueous phosphate buffer medium at pH 7.

Reductively induced stepwise replacement of chloride ligands by solvent molecules was proposed on the basis of the identification of the products of substitutions by using Lever's equation. Kinetic investigations by digital simulation

(63) Ni Dhubhghaill, O. M.; Hagen, W. R.; Keppler, B. K.; Lipponer, K. G.; Sadler, P. J. *J. Chem. Soc., Dalton Trans.* **1994**, 3305−3310.

of the cyclic voltammograms of these reactions revealed that an increase of the net electron donor character (decrease of E_L) of the neutral ligands (DMSO < indazole < triazole < imidazole) and of the basicity of the azole ligand promotes the complex lability toward the solvolytic dechlorination, but hampers the $Ru^{III} \rightarrow Ru^{II}$ reduction (shifts cathodically the reduction potential). Hence, a thermodynamic stabilization effect of the ligands on the Ru^{III} [relative to Ru^{II}] complexes is concomitant with the kinetic labilization of the corresponding reduced Ru^{II} forms.

Replacement of a Cl^- ligand by the solvent results in a positive shift of the reduction potential, and this fact should also be taken into account to design potential antitumor drugs able to follow the activation by the reduction pathway.

The slope, S_M, and intercept, I_M, of Lever's equation were also determined, for the first time, for the Ru^{III}/Ru^{IV} couple in organic medium, which will allow the prediction of the redox potential of other ruthenium systems with such a redox couple.

Although the generality of some of the above conclusions has still to be tested with a wider variety of ruthenium complexes, they are of significance for the understanding of the Ru^{III} reduction process which appears to play a key role in the activation of the ruthenium prodrugs in vivo. They can also be further applied to design ruthenium antitumor drugs with desired redox properties and chloride substitution lability, in biological systems, which currently constitutes quite a challenging task in the field of medicinal inorganic chemistry.

Acknowledgment. We are indebted to FWF (Austrian Science Fund), University of Vienna (Faculty of Sciences and Mathematics, International Relations Office), COST, the Foundation for Science and Technology and its POCTI-program (FEDER funded) (Portugal), and the European Community (contract MRTN-CT-2003-503864), for financial support. We also thank Prof. G. Giester for X-ray data collection and Dr. T. Weyhermüller for discussions of the crystallographic part of the work.

Note Added after ASAP: The version of this paper posted September 21, 2004, contained a number of errors, primarily in notation. Also, one value in Table 5 was incorrect. The version posted on September 23, 2004, has been corrected.

Supporting Information Available: X-ray crystallographic files in CIF format for **A2a**, **A2b**, **A3**, and **B3a**. Cyclic voltammograms of **A1** and **B3b** (pdf).This material is available free of charge via the Internet at http://pubs.acs.org.

IC049479C